Published in final edited form as:

Biomater Sci. 2019 January 29; 7(2): 560–570. doi:10.1039/c8bm01269e.

Polyester-based Ink Platform with Tunable Bioactivity for 3D Printing of Tissue Engineering Scaffolds

Shen Ji[a,$], **Koustubh Dube**[b,$], **Julian P. Chesterman**[b], **Stephanie L. Fung**[b], **Chya-Yan Liaw**[a], **Joachim Kohn**[b,*], and **Murat Guvendiren**[a,*]

[a]Otto H. York Chemical and Materials Engineering, New Jersey Institute of Technology, 161 Warren Street, Newark, NJ 07102, USA.

[b]New Jersey Center for Biomaterials, Rutgers University, 145 Bevier Rd., Piscataway, NJ 08854, USA.

[$]Co-1st Author

Abstract

In this work, we synthesized a novel polymeric biomaterial platform with tunable functionalizability for extrusion-based 3D printing. Biodegradable polymers were synthesized using 4-hydroxyphenethyl 2-(4-hydroxyphenyl)acetate (HTy), which is derived from Tyrosol and 2-(4-hydroxyphenyl)acetic acid. *p*-Phenylenediacetic acid (PDA) was introduced to enhance crystallinity. To enable functionalizability without deteriorating printability, glutamic acid derivatives were introduced into the polymer design, forming copolymers including poly(HTy-co-45%PDA-co-5%Gluhexenamide ester) (HP5GH), poly(HTy-co-45%PDA-co-5%Glupentynamide ester) (HP5GP), and poly(HTy-co-45%PDA-co-5%BocGlu ester) (HP5BG). The resulting polymers have: two melting temperatures (125–131 ˚C and 141–147 ˚C), Young's moduli of 1.9–2.4 GPa, and print temperatures of 170–190 ˚C. The molecular weight (M_w) loss due to hydrolytic degradation was gradual with~30% M_w retained after 25 weeks for HP5BG, whereas it was much faster for HP5GP and HP5GH with only 18% M_w retained after 8 weeks. HP5GH and HP5GP were successfully functionalized in solution (bulk) or on the surface using click-based chemistry. Finally, the utilization of this novel platform was demonstrated by studying osteogenic differentiation of human mesenchymal stem cells (hMSCs) using 3D printed scaffolds from HP5GP. Scaffolds were functionalized with azide-Heparin (az-Heparin) to bind and deliver bone morphogenetic protein 2 (BMP-2). This sample group significantly enhanced osteogenic differentiation of hMSCs as compared to unfunctionalized scaffolds incubated directly with az-Heparin or BMP-2 prior to cell culture. This novel polymer platform with tunable functionalizability could be utilized for additive manufacturing of biodegradable devices and scaffolds with tailored mechanical and bioactive properties for a wide range of medical applications including bone fixation devices and scaffolds for bone regeneration.

[*]Corresponding authors.

Conflicts of Interest

There are no conflicts to declare.

Electronic Supplementary Information (ESI) available: [details of any supplementary information available should be included here]. See DOI: 10.1039/x0xx00000x

Graphical Abstract

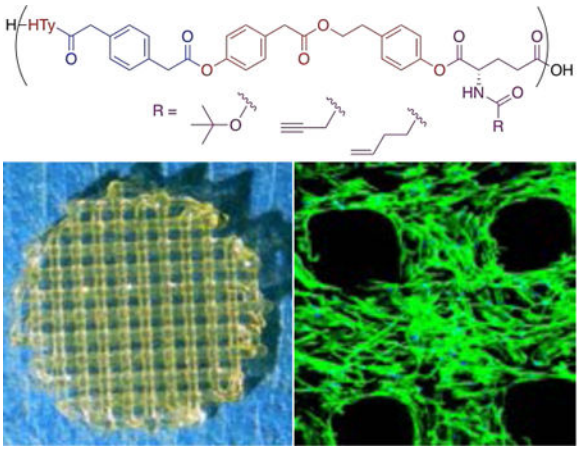

A novel polymeric biomaterial platform with tunable functionalizability for extrusion-based 3D printing.

1. Introduction

Over the last decade, 3D printing has become a promising manufacturing approach for a wide range of medical applications, including dentistry, tissue engineering and regenerative medicine, medical devices, anatomical models, and pharmaceutics.[1–3] 3D printing enables fabrication of custom-designed and patient-specific tissue engineering scaffolds and devices using the patient's own medical images, which is not possible with conventional scaffold fabrication techniques.[4–10] In addition, conventional techniques generally lack precise control of pore size, geometry, interconnectivity, spatial distribution, and the overall scaffold architecture.[11–13] These are crucial parameters for a biomaterial to promote the vascularization and tissue ingrowth that are necessary to establish functional integration of the scaffold.[14–17] However, the majority of devices currently printed using polymeric biomaterials only serve as a structural support; they permit, but do not promote, biological function.[18–19] This limitation is due to the lack of bioactivity of common printable polymers, such as poly(lactic acid) (PLA) and polycaprolactone (PCL). Due to their thermoplastic and semi-crystalline behaviour, PLA and PCL can be easily extruded as filaments for fused deposition (FDM) printing or directly printed from melt using direct ink writing (DIW). Semi-crystalline behaviour contributes to dimensional stability during melt to solid transition and to mechanical properties (stiffness). Both PLA and PCL are extensively used to 3D print tissue fixation devices and tissue engineering scaffolds, in particular for musculoskeletal tissue.[20–21] Although significant progress has been made to develop novel printable soft material platforms (including hydrogels and elastomeric systems),[22–29] the progress in biodegradable "stiff" polymers is very limited.

From a materials-perspective, a polymeric biomaterial should meet the requirements for printing to be considered an "ink". Rheological properties of the polymers are crucial to determine their printability. For extrusion-based printing, the polymer melt must flow at the print temperature (T_p) (usually below 250 ˚C for commercially available printers); thus, the

loss modulus (*G"*) must be greater than the storage modulus (G') at T_p.[30] The melt viscosity should be below 10^6 mPa.s to allow flow under applied pressure (usually ≤110 psi for commercially available printers).[31] In addition, the polymer must have a reversible and fast melt to solid phase transformation (within minutes) to rapidly melt in the hot nozzle and to rapidly solidify when extruded from the nozzle.[32]

In addition to printability, the ideal polymeric biomaterial should have sufficient mechanical properties (stiffness, toughness, etc.) to provide structural integrity, thereby enabling direct implantation, and should be biodegradable to allow replacement of the scaffold by newly grown tissue.[33–36] The latter requires the use of polymers that hydrolytically or enzymatically degrade to biocompatible, resorbable monomers that can be easily excreted from the body.

Finally, polymeric biomaterials often require bioactivity to control cell function, including cell migration (infiltration), proliferation, and phenotype preservation or differentiation.[37–40] Naturally occurring polymers usually display inherent bioactivity, which is not the case for synthetic polymers. Thus, it is of great interest to design functionalizable synthetic polymers for 3D printing. Polymers can be functionalized at the end groups or along the backbone by adding pendant reactive groups, such as carboxylic acids,[41] amines,[42] or hydroxyls.[43] One of the most commonly utilized approaches is click-based conjugation chemistry using click-ready pendant groups, such as alkenes, alkynes, azides, and epoxides.[44–45] Click chemistry has been employed for a wide range of applications including bioconjugation, labelling, surface functionalization, polymer synthesis and modification, and hydrogel modification.[44, 46–48]

In this study, we developed a novel platform of 3D printable biodegradable polymers with tunable bioactivity via click-based chemistry for extrusion-based printing, with printability and stiffness comparable to PLA. A wide range of tyrosine-derived polycarbonates with tunable properties have been developed previously.[49–53] In this work, the synthetic design was based on 4-hydroxyphenethyl 2-(4-hydroxyphenyl)acetate (HTy), which is an ester derived from Tyrosol and 2-(4-hydroxyphenyl)acetic acid. Both compounds are naturally occurring organic molecules found in olive oil.[54–55] HTy has been shown to be antioxidant, anti-stress, and antibacterial.[54–55] *p*-Phenylenediacetic acid (PDA) was incorporated into the synthetic design to tune thermal processability by enhancing crystallinity via **π-π** stacking interactions. To enable functionalizability, glutamic acid derivatives were incorporated into the synthetic design without deteriorating printability and stiffness. Glutamic acid is a diacid with a pendant amine group, which can be easily modified to incorporate various functional groups. In this study, we focused on alkyne and alkene functionality for commonly utilized click-based conjugation chemistry.

To demonstrate the utilization of this novel ink platform, osteogenic differentiation of stem cells was studied using 3D printed scaffolds. 3D printed scaffolds were functionalized with azide-Heparin (az-Heparin) via click chemistry. Heparin is a linear polysaccharide found in most biological tissues. Heparin is known to sequester growth factors, enzymes, and matrix proteins. Thus, it is extensively used for the sustained release of growth factors including bone morphogenetic protein-2 (BMP-2) (for up to 20 days)[56–57] to enhance bone

regeneration.[58] Our results showed a significant increase in osteogenic differentiation of stem cells when the scaffolds were tethered with heparin-bound BMP-2.

2. Experimental

Synthetic Procedures

Monomer Synthesis

Monomers including 4-hydroxyphenethyl 2-(4-hydroxyphenyl) acetate (HTy) (Scheme 1A), hex-5-enoylglutamic acid (Gluhexenamide) (Scheme 1B), and pent-4-ynoylglutamic acid (Glupentynamide) (Scheme 1C) were synthesized as described in the Experimental Section of the Supplementary Information.

Polymer Synthesis

A general procedure for the polymer synthesis (Scheme 2)is provided here and further details can be found in the Experimental Section of the Supplementary Information. In a round bottom flask, 1 equivalent of diol, 0.97 combined equivalents of diacid, and 0.33 equivalents of 1,4-dimethylpyridinium p-toluenesulfonate (DPTS) were combined with dichloromethane (DCM) and magnetically stirred for 15 min. The stirring reaction mixture was cooled for 30 min in an ice bath and then 2.1 equivalents of N,N′-diisopropylcarbodiimide (DIC) were added. The stirring reaction mixture was kept in an ice bath for 1 hour and then allowed to gradually warm to room temperature overnight. After 16 hours, the reaction mixture was precipitated by gradually adding isopropanol (5× DCM volume) while stirring. The precipitate was collected by vacuum filtration, redissolved in DCM, and reprecipitated using isopropanol, twice. The final precipitate was collected by vacuum filtration and dried in a vacuum oven at 40 ˚C for 48 hours.

Monomer and Polymer Characterization

The synthesized monomers and polymers were characterized by ^{1}H NMR spectroscopy using Varian 400 MHz and 500 MHz NMR spectrometers with dimethyl sulfoxide-d6 (DMSO-d6) as solvent and peak shifts referenced to an internal tetramethylsilane standard. The molecular weight of the monomers was determined by electrospray ionization-mass spectroscopy (ESI-MS, Thermo Finnigan LCQ Duo). The number average molecular weight (M_n), weight average molecular weight (M_w), and the molecular weight distribution of the polymers were determined using gel permeation chromatography using a Waters 2695 GPC apparatus with a guard and 2 columns. Samples were dissolved in HPLC grade dimethylformamide (DMF) at a 2 mg/mL concentration, filtered through a 0.2 μm syringe filter, and run at 25 °C using HPLC grade DMF with 0.1% trifluoroacetic acid (TFA) as the eluent. Molecular weights were calculated relative to polystyrene standards (M_w = 7.2–526 kDa).

Thermal Properties

Thermal properties including the glass transition temperature (T_g) and melting point (T_m) were determined by differential scanning calorimetry (DSC) from the second heating scan at a 10 ˚C/min heating rate using a Mettler Toledo DSC821. The thermal degradation of the

polymers was studied by thermogravimetric analysis (TGA, Mettler Toledo). The temperature at which mass loss began in the thermogram was considered as the thermal degradation temperature (T_d).

Compression Molding

Polymer films were fabricated using a Carver press (Carver 2625) at T_g+50 ˚C or T_m+10 ˚C. Briefly, 0.3 g of polymer powder was placed between two Kapton films in a preheated steel mold, placed in the Carver press, and compressed using 1000 psi. The thickness of the films was adjusted by using spacer shims.

Melt Rheology

Melt rheology (Kinexus Ultra$^+$, Malvern Instruments) was used to study solid to melt transition behaviour and temperature dependent melt viscosity of the polymers. Compression molded polymer films (500 μm in thickness) were tested using a 20 mm diameter plate at a constant frequency (1 Hz) with increasing temperature (1 ˚C/min) up to 200 ˚C. Storage modulus (G'), loss modulus (G"), and melt viscosity were recorded with increasing temperature. The solid to melt transition temperature was defined as the temperature where G'=G".

Mechanical Properties

Mechanical properties of the polymer films were tested using a mechanical tensile tester (MTS Sintech/5D Universal Testing Machine) with a 10 N load cell and a 10 mm/min displacement rate. The tensile Young's modulus was calculated from the slope of the tangent drawn at the linear portion of the stress strain curve (0 to 2%). Five samples of each polymer were tested. Compression tests were performed on 3D printed scaffolds (cylindrical specimens that are 5 mm in height and 9 mm in diameter) using an Instron machine (Instron model 3343) with a 1000 N load cell and a 0.5 mm/min displacement rate. Three samples of each polymer were tested.

Hydrolytic Degradation

Hydrolytic degradation was studied by incubating films (5 mm diameter discs) in 1 mL phosphate-buffered saline (PBS) with 0.01% sodium azide at 37 ˚C. The solution was changed weekly for the duration of the study. At each time point (every 3–4 days), three scaffolds were separated, washed with DI water, lyophilized, and characterized gravimetrically for loss in mass and by GPC for M_n and M_w.

Functionalizability

The reactivity of the polymers with glutamic acid derivatives was characterized in bulk (using polymer solutions) and/or on the surface (using compression molded films). 1*H*,1*H*,2*H*,2*H*-perfluorodecanethiol was used to investigate reactivity in the bulk and on the surface for HP5GH and in bulk for HP5GP. Surface reactivity for HP5GH and HP5GP was also investigated using bovine serum albumin (BSA) and az-Heparin, respectively. Az-Heparin was synthesized by reacting heparin with imidazole sulfonyl azide (azo transfer reagent) as described in the Supplementary Information.[59] Characterization was done by X-ray

photoelectron spectroscopy (XPS) for surface and ^{19}F NMR for bulk. A quartz crystal microbalance (Q-sense) was used to monitor the conjugation reaction of az-Heparin and physical adsorption of BMP-2 on polymer films in real time and the change in frequency was converted to a change in mass using the well-known Sauerbrey equation.[60]

3D Printing of Scaffolds

A 3D Bioplotter® Starter Series (EnvisionTEC GmbH, Germany) was used to print the scaffolds. The 3D digital model for the scaffolds was designed and saved as an STL file using Autodesk® Fusion 360™. The scaffold was designed as a solid cylinder (1 mm in height and 9 mm in diameter) to fit in a 48-well plate. Perfactory RP software was used to slice the STL file with 250 μm layer height. The sliced file was transferred to 3D Bioplotter® and a linear infill pattern with 0.75 mm spacing was created with alternating 0° and 90° rotation between layers. To begin printing, polymer powder was loaded into a stainless-steel syringe and heated to a printing temperature determined by the thermal properties of each polymer. Line tests were performed to determine the optimum printing parameters, including temperature, pressure, and speed. Briefly, a built-in line test protocol was used to print individual struts using a range of print pressures and speeds at a predefined print temperature. Print parameters were optimized to print struts with a 350 μm diameter. Scaffolds were characterized by scanning electron microscopy (SEM, Jeol).

Preparation of Scaffolds for Cell Culture

To investigate stem cell attachment and proliferation, two sets of scaffolds were printed from PLA, HP, HP5BG, HP5GP, and HP5GH. Scaffolds were sterilized by immersion in 75% ethanol for 30 min, followed by irradiation with a germicidal UV lamp for 1 h per side. After sterilization, one set was incubated with fibronectin from bovine plasma (20 μg/mL, Sigma), while the other set was incubated in Dulbecco's phosphate-buffered saline (DPBS). After the incubation solutions were aspirated, the scaffolds were rinsed with DPBS three times, transferred into non-treated 48-well plates, and maintained in 0.5 mL of growth media per well for 2 h prior to cell seeding.

For differentiation studies, 4 groups of HP5GP scaffolds were used. Two of the groups were functionalized with az-Heparin (HP5GP-Heparin) by incubating the scaffolds in 200 μL az-Heparin solution (0.15 μg/mL az-Heparin in DI water) with 10 μL of copper sulfate pentahydrate (45 mg/mL) and 10 μL of sodium ascorbate (112.5 mg/mL) for 24 h. The scaffolds were washed with PBS 3 times. One of these sample groups was further functionalized with recombinant human BMP-2 (Shanghai Rebone Biomaterials) (HP5GP-Heparin-BMP2) by incubating the scaffolds in 200 μL BMP-2 solution (7.5 μg/mL) for 1 h. One of the HP5GP groups was directly incubated with BMP-2 (7.5 μg/mL) for 1 h, washed with PBS (3×), and used as a control. All scaffold groups (HP5GP, HP5GP-Heparin, HP5GP-Heparin-BMP2, and HP5GP-BMP2) were transferred into growth media 2 h prior to cell seeding.

Cell Culture and Characterization

Human mesenchymal stem cells (hMSCs, Lonza) were cultured in growth media (α-MEM (minimum essential medium) supplemented with 10% fetal bovine serum (FBS, Gibco) and

1% penicillin streptomycin). hMSCs (115,000 cells/mL, passage 3) were seeded from the top surface (300 μL per scaffold corresponding to 12,500 cells/cm^2) and incubated at 37 ˚C for 60 min to allow for cell attachment. Scaffolds were gently turned upside down and hMSCs were seeded again (300 μL at 115,000 cells/mL) from the top. For cell attachment and proliferation studies, the cells were cultured for 14 days in growth media. For differentiation studies, after 2 days of culture in growth media, the media was replaced with osteogenic induction media (Lonza) and the cells were cultured up to 21 days. Media was refreshed every 3 days. For control studies with soluble BMP-2 ((+)sBMPs), 1 μL of BMP-2 solution (165 μg/mL in DI water) was added into the media with each media change.

An alamarBlue cell viability assay (Invitrogen) was used to investigate cell viability at 2, 4, 7, and 10 days of culture for each group (6 samples per group). To quantify double stranded DNA (dsDNA), Quant-iT™ PicoGreen™ dsDNA assay kit (Invitrogen) was used. For this purpose, 3 samples per group were collected at culture day 1, 4, 7, 10, and 14. The cells from each sample group were lysed and stored at −80 ˚C until all time points were collected for quantification. For both assays, an Infinite M200 Pro plate reader (Tecan) was used.

To visualize cells on the scaffolds, cells were washed with DPBS, fixed in 4% formalin for 15 min, and incubated in Triton X-100 solution (0.25% Triton X-100 in PBS) for 15 min to permeabilize the cell membrane. Cells were stained for F-actin using Alexa Fluor™ 488 Phalloidin (1:40 in PBS, Molecular Probes) and nuclei by 4′,6-diamidino-2-phenylindole (1:2000 in PBS, DAPI, Invitrogen). For differentiation studies, cells were stained for alkaline phosphatase (ALP) with Fast Blue RR/naphthol solution (Sigma), stained for calcium deposition with alizarin red (AR), or immunostained for osteocalcin (OC). For fluorometric quantification of AR staining, cells were de-stained using 10% cetylpyridinium chloride in 10 mL sodium phosphate (10 mM, pH 7). For immunostaining, cells were rinsed with PBS (3×) and incubated in blocking solution (10% goat serum in PBS) for 30 min after the permeabilization step. Samples were incubated with the OC primary antibody (1:200, monoclonal mouse, Fisher Scientific Co.) in staining solution (3% BSA, 0.1% Tween-20, 0.25% Triton-X) overnight at 4 ˚C. After washing with 3% BSA solution, cells were incubated in Alexa Fluor 488 rabbit anti-mouse secondary antibody (1:100, Fisher Scientific Co.) in a 3% BSA solution. Cells were imaged by confocal microscopy (confocal and 2-photon system, Leica). The nuclei of the OC and ALP stained cells were counted using ImageJ to determine OC and ALP positive cells.

Statistical Analysis

The data were analysed using KaleidaGraph. Data are presented as mean±standard deviation. ANOVA with Tukey's HSD post hoc test of means was used to make comparisons between sample groups. (n≥ 3 samples per group).

Results and Discussion

Monomer and Polymer Synthesis

The HTy monomer was synthesized via Fischer esterification from Tyrosol and 2-(4-hydroxyphenyl)acetic acid (Scheme 1A). HTy degrades hydrolytically to reform Tyrosol

and 2-(4-hydroxyphenyl)acetic acid. Since HTy contains phenyl rings, polymers that incorporate them tend to show semi-crystalline behaviour due to π-π stacking interactions. To enhance the π-π stacking interactions of HTy-containing polymers and hence their processability, *p*-phenylenediacetic acid (PDA) was introduced into the polymer design. Functionalizability was achieved by incorporating amide derivatives of glutamic acid (GR), which were synthesized by reacting the dimethyl ester of glutamic acid with alkene (Scheme 1B) or alkyne carboxylic acids(Scheme 1C). Alkene or alkyne functionality was chosen to enable click-chemistry for tethering bioactive cues. Poly(HTy-50%PDA) (HP), poly(HTy-45%PDA-co-HTy-5%Gluhexenamide) (HP5GH), poly(HTy-45%PDA-co-HTy-5%Glupentynamide) (HP5GP), and poly(HTy-45%PDA-co-HTy-5%BocGlu) (HP5BG) were successfully synthesized by condensation polymerization of selected combinations of HTy, PDA, and GR using DIC and DPTS as a catalyst (Scheme 2). Note that HTy undergoes 1:1 step growth reaction with PDA and GR during polymerization. Thus, the general formula for the functionalizable polymers is poly($HTy_{(0.5-x)}$-$PDA_{(0.5-x)}$-co-HTy_x-GR_x). Although we synthesized three polymer compositions with x = 0.01, 0.05, and 0.10, x=0.05 was used in this study due to favourable thermal properties, which will be discussed below. For simplicity, functionalizable polymers are referred to using the following format: HP5GR, where H, P, and GR denote HTy, PDA, and GR, and the number (5) indicates the mole percentage of functionalizable GR group. The M_w and *PDI* of each polymer are given in Table 1. NMR spectra are shown in ESI Figures S1-S5.

Thermal and Mechanical Characterization

Thermal properties of the polymers are summarized in Table 1. For poly(HTy carbonate) (p(HTy)), the T_g was observed at 54 ˚C. A shallow melting peak observed at 130 ˚C during the first heating cycle disappeared in the second heating cycle, thus indicating an amorphous behaviour. The lack of crystalline behaviour could be due to the rigidity of the carbonate bonds in the polymer backbone preventing the randomly oriented HTy repeating units from aligning for π-π stacking interactions. When PDA was incorporated into the polymer design to form HP, the T_g dropped slightly to 50 ˚C and two distinct melting transitions were observed at T_{m1} = 131 ˚C and at T_{m2} = 147 ˚C (Figure 1). Replacing the carbonate bonds with PDA increases backbone flexibility and the appearance of two melting points may indicate the presence of distinct crystalline regions formed by either HTy or PDA π-π stacking interactions. HP5BG, HP5GH, and HP5GP all have similar thermal properties to HP with T_g, T_{m1}, and T_{m2} values within 4–6 ˚C (Figure 1). All of the polymers decomposed at temperatures between 320–350 ˚C. Note that polymers containing 5 mole% GR were used in this study as the resulting polymer becomes amorphous for 10 mole% GR. The average tensile Young's modulus values of the polymers were in the range of 1.9 to 2.4 GPa with yield stress values from 28 to 40 MPa (Table 1). Both of these values were not statistically different when compared for each polymer.

Hydrolytic Degradation

Polyesters undergo hydrolytic degradation due to the ester bonds in their backbone. The hydrolytic degradation of compression molded polymer films (HP, HP5BG, HP5GP, and HP5GH) was studied at 37 ˚C in PBS (Figure 2). For HP, a steady decrease in M_w was observed between weeks 5 and 22, reaching undetectable M_w values after 22 weeks. For

HP5BG, a generally linear decrease in M_w was observed for the entire 25 week study. The M_w decreased much faster for HP5GP and HP5GH, such that only 18% M_w was retained after 8 weeks. We believe that this result could be due to less bulky side groups as compared to Boc in HP5BG. There are only a few semi-crystalline polymers that show a comparable high rate of degradation, such as poly(glycolic acid) (PGA) (degradation rate of 3–4 months).[61] There was no significant mass loss for HP and HP5BG, which could be due to the hydrophobic nature of the polymer limiting the solubility of the degraded chains (Figure 2B). The rate of mass loss for HP5GH and HP5GP was 3% and 2.5% per week, respectively. We did not observe any significant change in Young's modulus values of HP5GH and HP5GP up to 4 weeks (ESI Figure S6).

Functionalizability

In this study, three distinct polymers with pendant groups were developed. HP5GH and HP5GP have alkene and alkyne groups capable of click chemistry. The alkyne group can participate in copper-catalyzed alkyne-azide cycloaddition (CuAAC) reactions, which are utilized extensively in the literature.[44, 46–48] The alkene group can react with sulfhydryl containing compounds in the presence of a photoinitiator and UV light or via a Michael-type addition reaction.[62] HP5BG contains Boc-protected amine groups capable of carbodiimide chemistry, which also enable functionalization with a wide range of side chain derivatives to further tether bioactive cues.

The reactivity of the alkene-containing HP5GH was tested by using a small thiol-containing molecule (1H,1H,2H,2H-perfluorodecanethiol) and a large protein (BSA (66.5 kDa)), containing cysteine residues (Figure 3). The highly-fluorinated thiol enabled the study of the reactivity of the polymer in solution via ^{19}F NMR and the reactivity of the polymer surface (using compression molded films) via XPS. ^{19}F NMR showed that approximately 94% of the alkene bonds were converted to thioether bonds after UV irradiation in the presence of a photoinitiator, Irgacure 2959 (ESI Table S1). For the surface reaction, XPS data showed that the fluorine peak was only observed in the presence of UV light exposure, whereas the peak was missing for HP5GH sans UV exposure and for HP (without the pendent alkene group) with UV exposure (Figure 3A). The effects of thiol concentration, photoinitiator concentration, and UV irradiation time on the reaction yield for compression molded films were studied in detail, and the results are summarized in ESI Table S1. QCM studies indicated that 700 ng/cm^2 of BSA was chemically tethered onto the surface of HP5GH with UV exposure, which was significantly more than the 100 ng/cm^2 of BSA physically adsorbed onto the surface in the absence of UV exposure (Figure 3B).

The reactivity of the alkyne-containing HP5GP was studied via a CuAAC reaction using az-Heparin. The reaction was monitored in real-time by QCM. 1 μg/cm^2 of az-Heparin was found to be conjugated to the surface of the polymer within 1 hour (Figure 4). Although az-Heparin was found to adsorb onto HP5GP and HP (polymer without a reactive pendent group) in the absence of the catalyst, the amount of adsorbed az-Heparin was significantly lower: 480 ng/cm^2 for HP5GP and 100 ng/cm^2 for HP (ESI Figure S7). Heparin is known to bind and release growth factors such as bone morphogenetic protein-2 (BMP-2). To further investigate the activity of tethered heparin, we studied the interaction of it with BMP-2.

Approximately 1 μg/cm^2 of BMP-2 was found to bind to the heparinated polymer surface and remained bound after rinsing with PBS for 10 h, indicating a strong association of BMP-2 with heparin. The ionic interaction between the BMP-2 and heparin was disrupted when a surfactant (SDS) was introduced.

Rheological Characterization

The rheological properties of polymers are crucial to determine their printability. For extrusion-based printing at elevated temperatures, the polymer melt must flow at the print temperature (T_p); thus, the loss modulus (G'') must be greater than the storage modulus (G') at T_p. In addition, the polymer must have a fast melt to solid phase transformation (within minutes) to rapidly melt in the hot nozzle and rapidly solidify when extruded from the nozzle.[30, 32] For instance, PLA, the most widely used polymer in 3D printing, shows a fast phase transformation, indicated by a sharp drop in G' within a very narrow temperature window (Figure 5). For commercial PLA, solid to melt transition occurred at T_{sm} = 180 ˚C and melt viscosity was equal to 8.4×10^5 mPa.s above 180 ˚C (usual printing temperature). For p(HTy), T_{sm} = 140 ˚C, with a shallow drop in G' and a relatively high melt viscosity value (η = 5×10^6 mPa.s). For HP, η was significantly reduced to 5×10^5 mPa.s with a significant drop in G' during solid-to-melt transition (at T_{sm} = 150 ˚C) (Figure 5), which is consistent with the impact of incorporating PDA on the thermal properties. Note that the melt rheological behaviour of HP was similar to PLA. Functionalizable polymers showed extended transition regions with T_{sm} = 150 ˚C, 140 ˚C, and 138 ˚C, and η = 3.3×10^2 mPa.s, 1.8×10^3 mPa.s, and 2.4×10^3 mPa.s (measured at 180 ˚C), for HP5BG, HP5GH, and HP5GP, respectively (Figure 5). This result could be due to hydrogen bonding interactions between the amide groups present in the glutamic acid derivatives. The melt rheological data for all polymers are given in Table 1.

3D Printing

An EnvisionTEC 3D Bioplotter®, an extrusion-based printer, was used to print the polymers. Initial extrusion tests were performed to determine the lowest print temperature (T_p) and polymer incubation time to equilibrate the print temperature (t_e). Following this study, printing parameters including print pressure (P) and print speed (v_p) were determined by performing line tests using two needle sizes. The summary of printing parameters to create 350 μm diameter print lines (struts) is given in Table 2. 3D scaffolds printed from HP, HP5BG, HP5GP, and HP5GH showed identical resolution when compared with scaffolds printed from PLA (Figure 6). In this study, we printed cylindrical scaffolds up to 5 mm in height and 9 mm in diameter, but the maximum height of the scaffold is determined by the printing method. We were able to print large constructs when we printed filaments using fused depositon modelling (not shown in this study), but for bioplotter the maximum size is limited to the amount of material that can be loaded into the metal syringe. SEM images showed self-supporting scaffolds constructed from uniform 350 μm diameter struts. Young's modulus values of the scaffolds were not significantly different from each other and in the range of 91–106 MPa (ESI Figure S7).

Stem Cell Culture and Osteogenic Differentiation

Human mesenchymal stem cells were cultured on 3D printed scaffolds for up to 14 days. Cells showed gradually increasing metabolic activity for the first 10 days, and total cell number (measured by dsDNA content) increased gradually starting from days 4 and 7 (Figure 7). Confocal images of the scaffolds at day 14 showed that cells had attached and spread uniformly to cover the struts (Figure 7C).

To utilize our functionalizable polymeric biomaterial ink platform, we studied the effect of heparin-tethered BMP-2 on osteogenic differentiation of hMSCs in osteogenic induction media for 21 days. For this purpose, we printed scaffolds from HP5GP and functionalized them with az-Heparin ((+)Hep). One set of the (+)Hep group was then tethered with BMP-2 ((+)Hep-BMP2). Unfunctionalized HP5GP was used as a negative control. In addition, we included a positive control group where soluble BMP-2 ((+)sBMP2) was introduced into the media during media changes. Cells were stained for OC (Figure 8A) and ALP (figure8B) as markers of osteogenic differentiation. Alizarin Red (AR) staining was also used to qualitatively and quantitatively determine calcium deposition. When the cells were quantified at day 14, 85±3% and 80±4% of the cells cultured in the (+)Hep-BMP2 and (+)sBMP2 groups, respectively, stained positive for OC, which were significantly higher than those cultured in the (+)BMP2 (68±4%), (+)Hep (58±6%), and HP5GP (56±8%) groups. At day 21, 93±4% and 100±5% of the cells in the (+)Hep-BMP2 and sBMP2 groups were OC-positive, compared to those in the (+)BMP2 (77±18%), (+)Hep (57±4%), and HP5GP (62±4%) groups. Increased expression of OC suggested osteogenic differentiation was upregulated when HP5GP was functionalized with Heparin-BMP2 (Figure8C). The (+)Hep-BMP2 group also showed significantly higher ALP-positive cells (57±3%) as compared to other groups at day 14 (Figure8D). When calcium deposition was characterized using AR staining, AR concentration increased significantly from~0.1 to 0.5 mM for 14- and 21-day culture respectively, yet the sample groups did not show any significant differences (Figure8E). A longer culture period may be required to see significant changes.

Conclusions

We used a bottom-up synthetic design approach to develop novel 3D printable polymeric biomaterials for extrusion-based printing from biodegradable stiff polymers with tunable functionalizability. The polymer designs were based on the hydrolytically degradable monomer HTy, which is synthesized from two naturally occurring olive oil components (Tyrosol and 2-(4-hydroxyphenyl)acetic acid). Despite the presence of phenyl rings, p(HTy) was generally amorphous and not printable using commercially available 3D printers. Introducing PDA into the synthetic design resulted in the HP copolymer, which showed crystalline behaviour due to enhanced **π-π** stacking interactions. The thermal processing properties of HP were almost identical to PLA, the gold standard for extrusion-based printing for biomedical applications. Functionalizability was achieved by incorporating glutamic acid derivatives (GR) into the synthetic design and generating copolymers of HTy, PDA, and GR. Our results showed that 5 mole% of GR addition did not significantly alter thermal properties, stiffness, and printability of these polymers. In this study, we particularly

focused on functionalizable polymers enabling click-based conjugation chemistry via alkyne (HP5GP) or alkene (HP5GH) functionality. We successfully demonstrated the reactivity of these functional groups in bulk (using polymer solutions) and on the surface (using polymer films). 3D scaffolds fabricated from these polymers showed uniform strut distribution within the scaffolds, with strut resolution identical to that of PLA. When cultured on these scaffolds, hMSCs were highly viable, and uniformly attached and spread on the struts. To further demonstrate the utility of the functionalizable polymers, we studied the osteogenic differentiation of hMSCs on HP5GP scaffolds functionalized with az-Heparin and BMP-2 ((+)Hep-BMP2). Our results showed a significantly higher fraction of the hMSCs stained positive for ALP and OC, which are osteogenic markers for stem cells.

Supplementary Material

Refer to Web version on PubMed Central for supplementary material.

Acknowledgements

This study is funded by the National Science Foundation under award number DMR-1714882 and by the National Institute of Health, National Institute of Biomedical Imaging and Bioengineering Award Number P41EB001046. We acknowledge Professor Changsheng Liu of East China University of Science and Technology (ECUST) for providing the BMP-2 used in this study.

Notes and References

1. Ji S; Guvendiren M, Recent Advances in Bioink Design for 3D Bioprinting of Tissues and Organs. Frontiers in Bioengineering and Biotechnology 2017, 5, 23. [PubMed: 28424770]
2. Liaw C-Y; Guvendiren M, Current and emerging applications of 3D printing in medicine. Biofabrication 2017, 9 (2), 024102. [PubMed: 28589921]
3. Murphy SV; Atala A, 3D bioprinting of tissues and organs. Nat. Biotechnol. 2014, 32 (8), 773–785. [PubMed: 25093879]
4. Billiet T; Vandenhaute M; Schelfhout J; Van Vlierberghe S; Dubruel P, A review of trends and limitations in hydrogel-rapid prototyping for tissue engineering. Biomaterials 2012, 33 (26), 6020–6041. [PubMed: 22681979]
5. Fedorovich NE; Alblas J; Hennink WE; Oner FC; Dhert WJA, Organ printing: the future of bone regeneration? Trends in Biotechnology 2011, 29 (12), 601–606. [PubMed: 21831463]
6. Marga F; Jakab K; Khatiwala C; Shepherd B; Dorfman S; Hubbard B; Colbert S; Gabor F, Toward engineering functional organ modules by additive manufacturing. Biofabrication 2012, 4 (2).
7. Ozbolat IT; Yu Y, Bioprinting Toward Organ Fabrication: Challenges and Future Trends. Ieee Transactions on Biomedical Engineering 2013, 60 (3), 691–699. [PubMed: 23372076]
8. Peltola SM; Melchels FPW; Grijpma DW; Kellomaki M, A review of rapid prototyping techniques for tissue engineering purposes. Annals of Medicine 2008, 40 (4), 268–280. [PubMed: 18428020]
9. Sun W; Darling A; Starly B; Nam J, Computer-aided tissue engineering: overview, scope and challenges. Biotechnology and Applied Biochemistry 2004, 39, 29–47. [PubMed: 14563211]
10. Kang HW; Lee SJ; Ko IK; Kengla C; Yoo JJ; Atala A, A 3D bioprinting system to produce human-scale tissue constructs with structural integrity. Nature Biotechnology 2016, 34 (3), 312-+.
11. Hollister SJ, Porous scaffold design for tissue engineering. Nature Materials 2005, 4 (7), 518–524. [PubMed: 16003400]
12. Hutmacher DW, Scaffold design and fabrication technologies for engineering tissues - state of the art and future perspectives. Journal of Biomaterials Science-Polymer Edition 2001, 12 (1), 107–124. [PubMed: 11334185]
13. Karageorgiou V; Kaplan D, Porosity of 3D biomaterial scaffolds and osteogenesis. Biomaterials 2005, 26 (27), 5474–5491. [PubMed: 15860204]

14. Miller JS; Stevens KR; Yang MT; Baker BM; Nguyen D-HT; Cohen DM; Toro E; Chen AA; Galie PA; Yu X; Chaturvedi R; Bhatia SN; Chen CS, Rapid casting of patterned vascular networks for perfusable engineered three-dimensional tissues. Nature Materials 2012, 11 (9), 768–774. [PubMed: 22751181]
15. Kolesky DB; Truby RL; Gladman AS; Busbee TA; Homan KA; Lewis JA, 3D Bioprinting of Vascularized, Heterogeneous Cell-Laden Tissue Constructs. Advanced Materials 2014, 26 (19), 3124–3130. [PubMed: 24550124]
16. Kolesky DB; Homan KA; Skylar-Scott MA; Lewis JA, Three-dimensional bioprinting of thick vascularized tissues. Proceedings of the National Academy of Sciences 2016, 113 (12), 3179.
17. Badylak SF; Weiss DJ; Caplan A; Macchiarini P, Engineered whole organs and complex tissues. Lancet 2012, 379 (9819), 943–952. [PubMed: 22405797]
18. Parthasarathy J, 3D modeling, custom implants and its future perspectives in craniofacial surgery. Annals of maxillofacial surgery 2014, 4 (1), 9–18. [PubMed: 24987592]
19. Zopf DA; Hollister SJ; Nelson ME; Ohye RG; Green GE, Bioresorbable Airway Splint Created with a Three-Dimensional Printer. New England Journal of Medicine 2013, 368 (21), 2043–2045. [PubMed: 23697530]
20. Woodruff MA; Hutmacher DW, The return of a forgotten polymer—Polycaprolactone in the 21st century. Progress in Polymer Science 2010, 35 (10), 1217–1256.
21. Serra T; Planell JA; Navarro M, High-resolution PLA-based composite scaffolds via 3-D printing technology. Acta Biomaterialia 2013, 9 (3), 5521–5530. [PubMed: 23142224]
22. Feinberg A; Hinton T Additive manufacturing of embedded materials. US20160167312A1,
23. Highley Christopher B; Rodell Christopher B; Burdick Jason A, Direct 3D Printing of Shear-Thinning Hydrogels into Self-Healing Hydrogels. Advanced Materials 2015, 27 (34), 5075–5079. [PubMed: 26177925]
24. Hinton TJ; Hudson A; Pusch K; Lee A; Feinberg AW, 3D Printing PDMS Elastomer in a Hydrophilic Support Bath via Freeform Reversible Embedding. ACS Biomaterials Science & Engineering 2016, 2 (10), 1781–1786. [PubMed: 27747289]
25. Hinton TJ; Jallerat Q; Palchesko RN; Park JH; Grodzicki MS; Shue H-J; Ramadan MH; Hudson AR; Feinberg AW, Three-dimensional printing of complex biological structures by freeform reversible embedding of suspended hydrogels. Science Advances 2015, 1 (9).
26. Govindarajan SR; Xu Y; Swanson JP; Jain T; Lu Y; Choi J-W; Joy A, A Solvent and Initiator Free, Low-Modulus, Degradable Polyester Platform with Modular Functionality for Ambient-Temperature 3D Printing. Macromolecules 2016, 49 (7), 2429–2437.
27. Yi-Cheun Y; Christopher BH; Liliang O; Jason AB, 3D printing of photocurable poly(glycerol sebacate) elastomers. Biofabrication 2016, 8 (4), 045004. [PubMed: 27716633]
28. Rutz AL; Hyland KE; Jakus AE; Burghardt WR; Shah RN, A Multimaterial Bioink Method for 3D Printing Tunable, Cell-Compatible Hydrogels. Advanced Materials 2015, 27 (9), 1607–1614. [PubMed: 25641220]
29. O'Bryan CS; Bhattacharjee T; Hart S; Kabb CP; Schulze KD; Chilakala I; Sumerlin BS; Sawyer WG; Angelini TE, Self-assembled micro-organogels for 3D printing silicone structures. Science Advances 2017, 3 (5).
30. Guvendiren M; Molde J; Soares RMD; Kohn J, Designing Biomaterials for 3D Printing. ACS Biomaterials Science & Engineering 2016, 2 (10), 1679–1693.
31. Mackay ME; Swain ZR; Banbury CR; Phan DD; Edwards DA, The performance of the hot end in a plasticating 3D printer. Journal of Rheology 2017, 61 (2), 229–236.
32. Anitha R; Arunachalam S; Radhakrishnan P, Critical parameters influencing the quality of prototypes in fused deposition modelling. Journal of Materials Processing Technology 2001, 118 (1–3), 385–388.
33. Engelberg I; Kohn J, Physicomechanical Properties of Degradable Polymers used in Medical Applications - a comparative-study. Biomaterials 1991, 12 (3), 292–304. [PubMed: 1649646]
34. Freed LE; Vunjaknovakovic G; Biron RJ; Eagles DB; Lesnoy DC; Barlow SK; Langer R, Biodegradable Polymer Scaffolds for Tissue Engineering. Bio-Technology 1994, 12 (7), 689–693. [PubMed: 7764913]

35. Huebsch N; Mooney DJ, Inspiration and application in the evolution of biomaterials. Nature 2009, 462 (7272), 426–432. [PubMed: 19940912]
36. Mitragotri S; Lahann J, Physical approaches to biomaterial design. Nature Materials 2009, 8 (1), 15–23. [PubMed: 19096389]
37. Mieszawska AJ; Kaplan DL, Smart biomaterials - regulating cell behavior through signaling molecules. BMC Biology 2010, 8, 59–59. [PubMed: 20529238]
38. Kohn J, New approaches to biomaterials design. Nature Materials 2004, 3 (11), 745–747. [PubMed: 15516948]
39. Guvendiren M; Burdick JA, Engineering synthetic hydrogel microenvironments to instruct stem cells. Current Opinion in Biotechnology 2013, 24 (5), 841–846. [PubMed: 23545441]
40. Ravi S; Chaikof EL, Biomaterials for vascular tissue engineering. Regenerative Medicine 2009, 5 (1), 107–120.
41. Kimura Y; Shirotani K; Yamane H; Kitao T, Ring-opening polymerization of 3(S)-[(benzyloxycarbonyl)methyl]-1,4-dioxane-2,5-dione: a new route to a poly(.alpha.-hydroxy acid) with pendant carboxyl groups. Macromolecules 1988, 21 (11), 3338–3340.
42. Trollsås M; Lee VY; Mecerreyes D; Löwenhielm P; Möller M; Miller RD; Hedrick JL, Hydrophilic Aliphatic Polyesters: Design, Synthesis, and Ring-Opening Polymerization of Functional Cyclic Esters. Macromolecules 2000, 33 (13), 4619–4627.
43. Tian D; Dubois P; Jérôme R, Macromolecular Engineering of Polylactones and Polylactides. 22. Copolymerization of ε-Caprolactone and 1,4,8-Trioxaspiro[4.6]-9-undecanone Initiated by Aluminum Isopropoxide. Macromolecules 1997, 30 (9), 2575–2581.
44. Adzima BJ; Tao Y; Kloxin CJ; DeForest CA; Anseth KS; Bowman CN, Spatial and temporal control of the alkyne–azide cycloaddition by photoinitiated Cu(II) reduction. Nature Chemistry 2011, 3, 256.
45. Ossipov DA; Hilborn J, Poly(vinyl alcohol)-Based Hydrogels Formed by “Click Chemistry”. Macromolecules 2006, 39 (5), 1709–1718.
46. DeForest CA; Anseth KS, Cytocompatible Click-based Hydrogels with Dynamically-Tunable Properties Through Orthogonal Photoconjugation and Photocleavage Reactions. Nature chemistry 2011, 3 (12), 925–931.
47. Link AJ; Tirrell DA, Cell Surface Labeling of Escherichia coli via Copper(I)-Catalyzed [3+2] Cycloaddition. Journal of the American Chemical Society 2003, 125 (37), 11164–11165. [PubMed: 16220915]
48. Speers AE; Adam GC; Cravatt BF, Activity-Based Protein Profiling in Vivo Using a Copper(I)-Catalyzed Azide-Alkyne [3 + 2] Cycloaddition. Journal of the American Chemical Society 2003, 125 (16), 4686–4687. [PubMed: 12696868]
49. Ertel SI; Kohn J, Evaluation of a series of tyrosine-derived polycarbonates as degradable biomaterials. Journal of Biomedical Materials Research 1994, 28 (8), 919–930. [PubMed: 7983090]
50. Sommerfeld SD; Zhang Z; Costache MC; Vega SL; Kohn J, Enzymatic Surface Erosion of High Tensile Strength Polycarbonates Based on Natural Phenols. Biomacromolecules 2014, 15 (3), 830–836. [PubMed: 24432806]
51. Tangpasuthadol V; Pendharkar SM; Kohn J, Hydrolytic degradation of tyrosine-derived polycarbonates, a class of new biomaterials. Part I: Study of model compounds. Biomaterials 2000, 21 (23), 2371–2378. [PubMed: 11055284]
52. Bourke SL; Kohn J, Polymers derived from the amino acid l-tyrosine: polycarbonates, polyarylates and copolymers with poly(ethylene glycol). Advanced Drug Delivery Reviews 2003, 55 (4), 447–466. [PubMed: 12706045]
53. Lewitus D; Smith KL; Shain W; Kohn J, Ultrafast resorbing polymers for use as carriers for cortical neural probes. Acta Biomaterialia 2011, 7 (6), 2483–2491. [PubMed: 21345383]
54. Papadopoulos G; Boskou D, Antioxidant effect of natural phenols on olive oil. Journal of the American Oil Chemists’ Society 1991, 68 (9), 669–671.
55. Aissa I; Bouaziz M; Frikha F; Mansour RB; Gargouri Y, Synthesized tyrosyl hydroxyphenylacetate, a novel antioxidant, anti-stress and antibacterial compound. Process Biochemistry 2012, 47 (12), 2356–2364.

56. Ruel M; Laham RJ; Parker JA; Post MJ; Ware JA; Simons M; Sellke FW, Long-term effects of surgical angiogenic therapy with fibroblast growth factor 2 protein. The Journal of thoracic and cardiovascular surgery 2002, 124 (1), 28–34. [PubMed: 12091805]

57. Jeon O; Song SJ; Kang S-W; Putnam AJ; Kim B-S, Enhancement of ectopic bone formation by bone morphogenetic protein-2 released from a heparin-conjugated poly (L-lactic-co-glycolic acid) scaffold. Biomaterials 2007, 28 (17), 2763–2771. [PubMed: 17350678]

58. Belair DG; Le NN; Murphy WL, Design of Growth Factor Sequestering Biomaterials. Chemical communications (Cambridge, England) 2014, 50 (99), 15651–15668.

59. van Dongen SF; Teeuwen RL; Nallani M; van Berkel SS; Cornelissen JJ; Nolte RJ; van Hest JC, Single-step azide introduction in proteins via an aqueous diazo transfer. Bioconjugate chemistry 2008, 20 (1), 20–23.

60. Guvendiren M; Brass DA; Messersmith PB; Shull KR, Adhesion of DOPA-Functionalized Model Membranes to Hard and Soft Surfaces. The Journal of Adhesion 2009, 85 (9), 631–645. [PubMed: 21461121]

61. Sheikh Z; Najeeb S; Khurshid Z; Verma V; Rashid H; Glogauer M, Biodegradable Materials for Bone Repair and Tissue Engineering Applications. Materials 2015, 8 (9), 5744–5794. [PubMed: 28793533]

62. Slavin S; Burns J; Haddleton DM; Becer CR, Synthesis of glycopolymers via click reactions. European Polymer Journal 2011, 47 (4), 435–446.

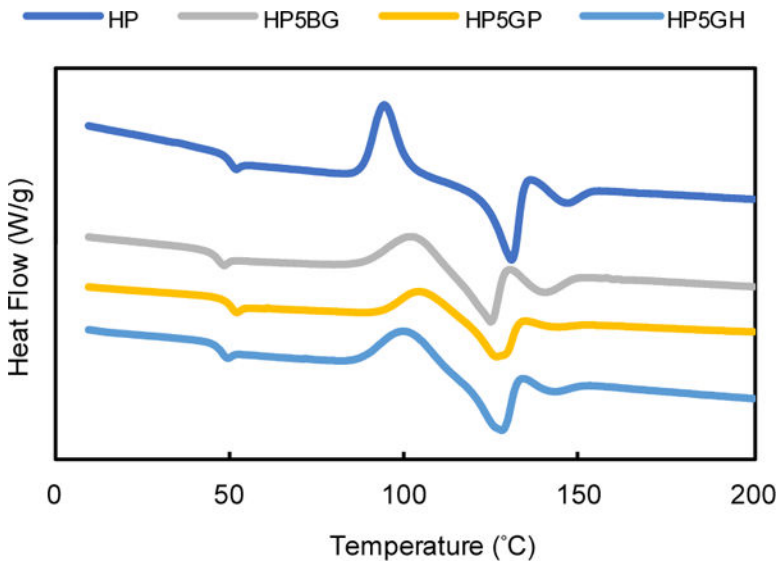

Figure 1.
DSC thermograms for the polymers.

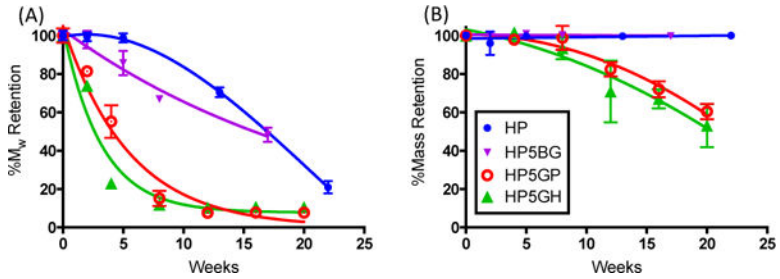

Figure 2.

Hydrolytic degradation of polymers over 25 weeks at 37 ˚C in PBS. (A) Percent retained molecular weight (%M_w) with time. (B) Percent mass retention with time.

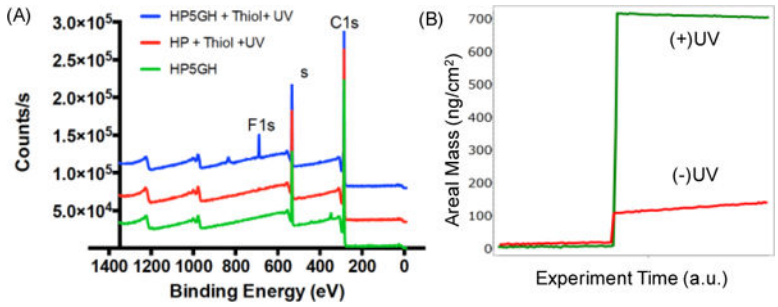

Figure 3.

(A) XPS spectra for HP5GH (green), HP reacted with 1*H*,1*H*,2*H*,2*H*-perfluorodecanethiol under UV light (red), and HP5GH reacted with 1*H*,1*H*,2*H*,2*H*-perfluorodecanethiol under UV light (blue). (B) QCM data showing the change in areal mass with time for HP5GH covered with BSA solution in the presence (+) or absence (−) of UV light.

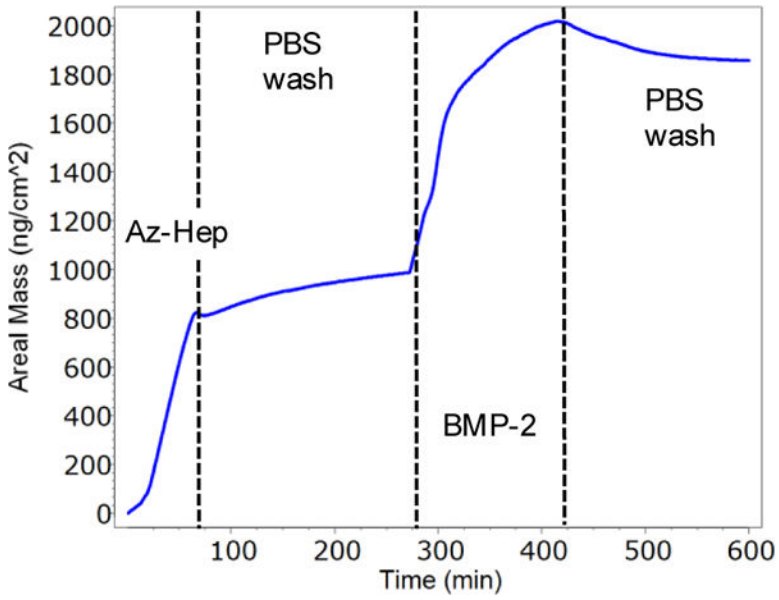

Figure 4.

QCM data showing the change in frequency with time for HP5GP. Az-Heparin was flowed over HP5GP film for 60 min, followed by PBS for 240 min, then BMP-2 for 100 min, and finally PBS.

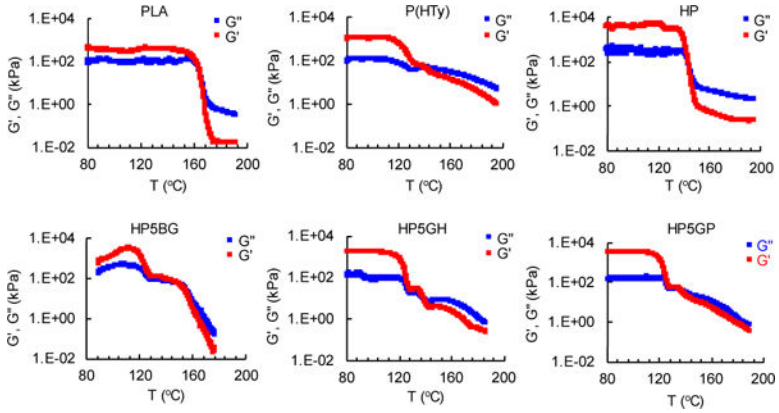

Figure 5.

Plots showing the change in storage modulus (G') and loss modulus (G") of the polymers with temperature (T). Solid to melt transition temperature is defined as the temperature where G'=G".

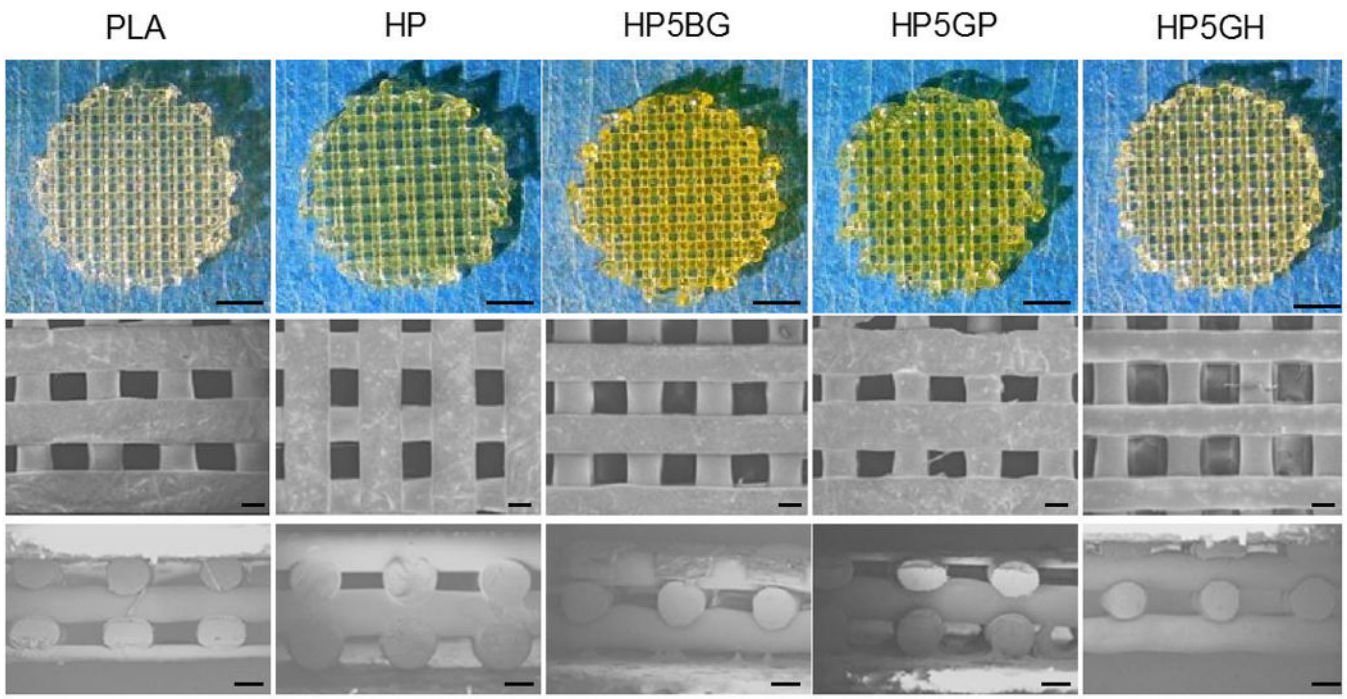

Figure 6.

Top row: 3D printed scaffolds from PLA, HP, HP5BG, HP5GP, and HP5GH. Middle row: The corresponding SEM images including from top view and cross-section are shown in middle and bottom row, respectively. Scale bars are 2 mm for top row and 200 μm for the SEM images.

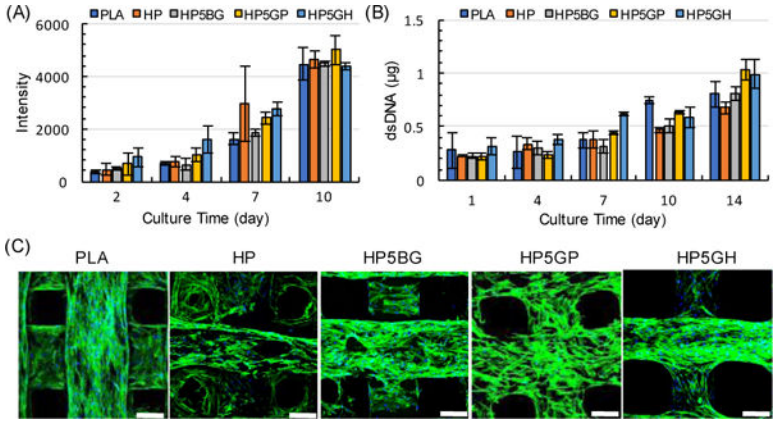

Figure 7.

A) Average peak intensities from alamarBlue cell viability assay for hMSCs cultured on scaffolds. B) Average dsDNA quantities found within each scaffold group. Error bars represent the standard deviation (n = 6 and 3 samples/group for A and B, respectively). C) Scanning fluorescent confocal 3D reconstructions of F-actin (green) and DAPI (blue) stained hMSCs cultured on the scaffolds for 14 days. Scale bars are 200 μm.

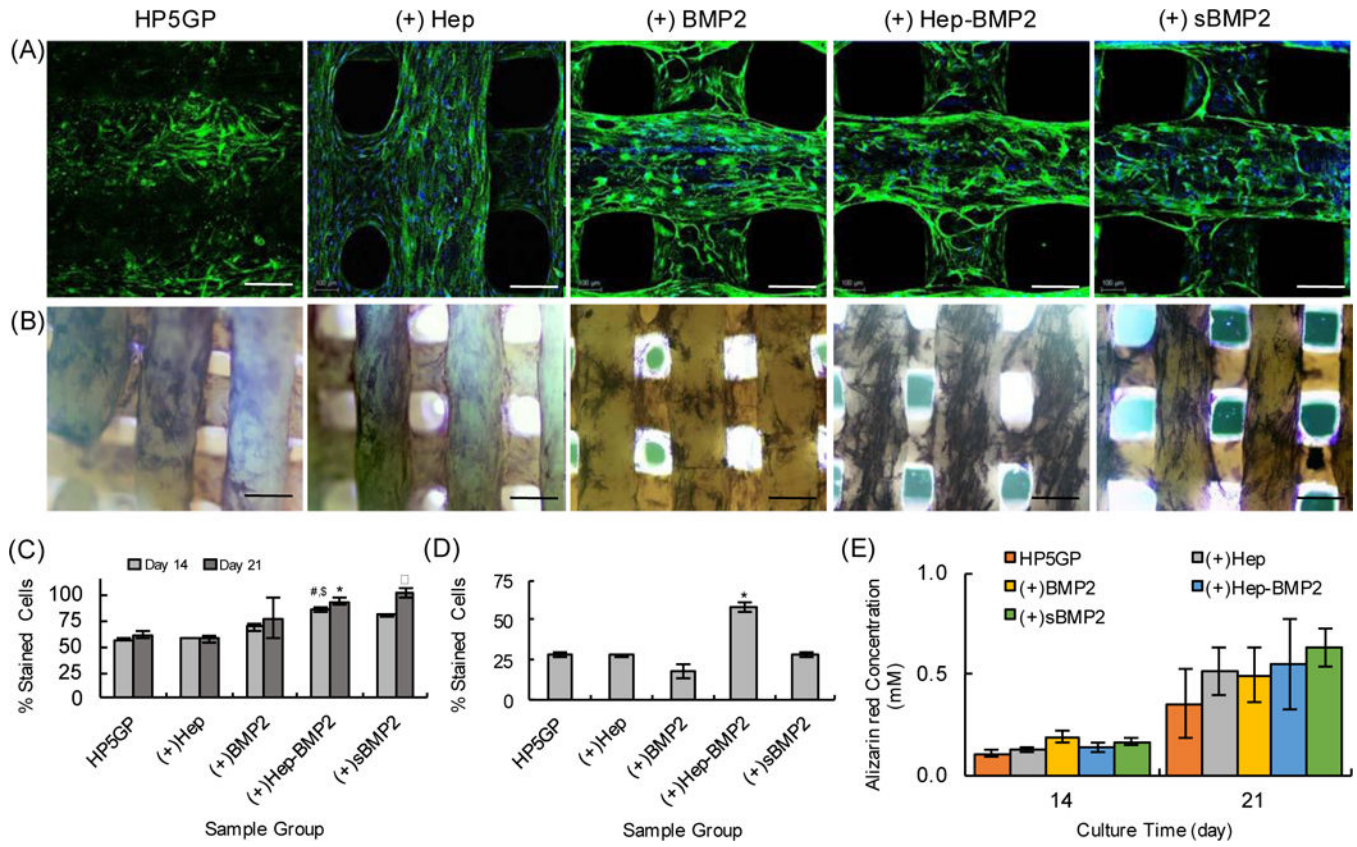

Figure 8.

A) Confocal images of hMSCs cultured on 3D printed scaffolds for 14 days in osteogenic differentiation media, and immunostained for human osteocalcin (OC) (green). Cell nuclei are stained with DAPI (blue). Scale bars are 200 μm. B) Brightfield images of hMSCs stained for alkaline phosphatase (ALP, dark blue/purple) after 14 days of culture in osteogenic media. Scale bars are 400 μm. C) Percentage of cells stained positive for OC corresponding to (A). For day 14, $^{\#}p<0.2$ for Hep-BMP2 as compared to HP5GP and (+)Hep, $^{\$}p<0.5$ for Hep-BMP2 as compared to (+)BMP2. For day 21, $^{\alpha}p<0.02$ sBMP2 group as compared to HP5GP, (+)Hep, and (+)BMP2, and $^{*}p<0.4$ for (+)Hep-BMP2 as compared to HP5GP and (+)Hep. D) Percentage of cells stained positive for ALP corresponding to (B). $^{*}p<0.001$ for (+)Hep-BMP2 as compared to other sample groups (n=3). E) Alizarin Red (AR) staining quantification results using fluorometric analysis depicting AR concentration (mM) for each scaffold after 14 and 21 days of culture in osteogenic induction media.

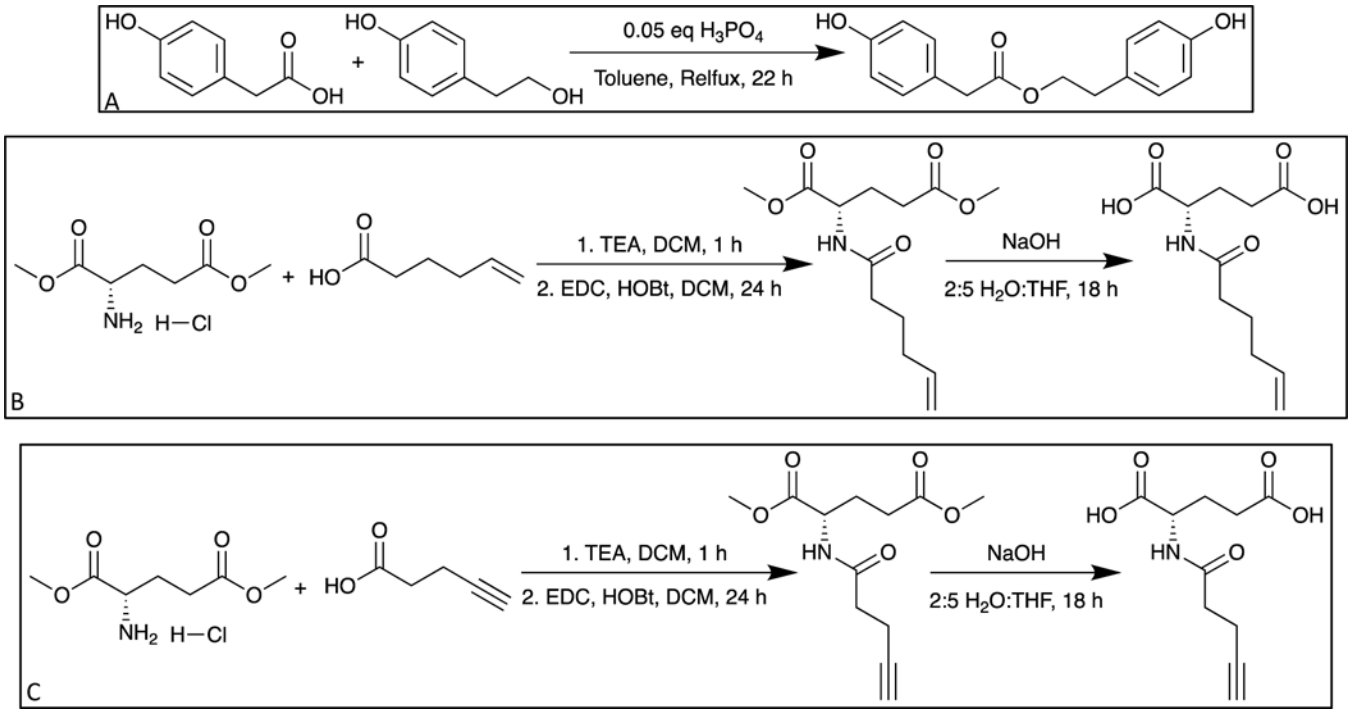

Scheme 1.

(A) Synthesis of HTy. (B) Synthesis of Gluhexenamide. (C) Synthesis of Glupentyamide.

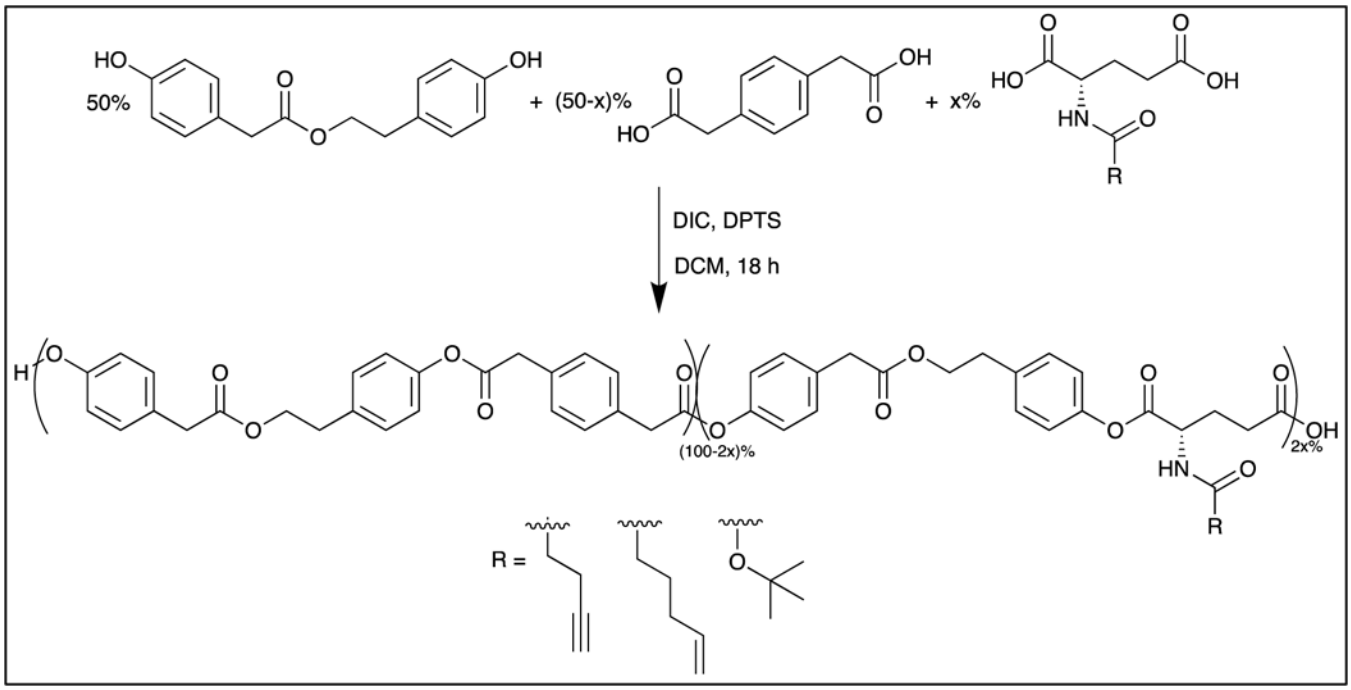

Scheme 2.
General polymer synthesis

Table 1.

Properties of the polymers.

Polymer	M_w [a] (kDa)	PDI[a]	T_g [b] (°C)	T_{m1} [b] (°C)	T_{m2} [b] (°C)	T_D [c] (°C)	E_T [d] (GPa)	σ_y [d] (MPa)	η [e] (mPa.s)	G' Fold Change[e]	%M_w Retention[f]
p(HTy)	181	1.8	54	-	-	350	2.4(±0.3)	38(±7)	5×10^6	1.1	-
HP	143	1.7	50	131	147	320	2.1(±0.3)	28(±3)	5×10^5	3.5	88
HP5BG	141	1.7	46	125	141	330	1.9(±0.1)	40(±3)	3.3×10^2	4.0	70
HP5GH	126	1.6	47	128	143	320	2.2(±0.1)	34(±6)	1.8×10^3	4.0	18
HP5GP	129	1.6	50	127	144	320	2.3(±0.1)	38(±2)	2.4×10^3	4.0	18

[a] From DMF GPC, relative to polystyrene standards.

[b] From DSC measurements.

[c] From TGA.

[d] From tensile tests using compression molded films.

[e] From melt rheology using compression molded films (η measured at 180 °C).

[f] From hydrolytic degradation tests (8 week point) using DMF GPC.

Table 2.

Printing parameters, including needle diameter (d), print temperature (T_p), time to equilibrate temperature (t_e), print pressure (P), and print speed (ν_π).

Polymer	d (mm)	T_p (°C)	t_e (h)	P (bar)	ν_p (mm/s)
PLA	0.3	200	0.5	7	2
HP	0.3	190	1	7	2
HP5BG	0.3	170	1	7	2
	0.4	170	1	6	13
HP5GH	0.3	170	1	7	3
HP5GP	0.3	175	0.5	7	1.5
	0.4	175	1	6	4